Results in Chemistry 5 (2023) 100766

Contents lists available at ScienceDirect

Results in Chemistry

journal homepage: www.sciencedirect.com/journal/results-in-chemistry

Charcoal activated as template Mg/Al layered double hydroxide for selective adsorption of direct yellow on anionic dyes

Nur Ahmad [a], Fitri Suryani Arsyad [a], Idha Royani [a], Aldes Lesbani [a,b,*]

[a] Graduate School, Faculty of Mathematics and Natural Sciences, Sriwijaya University, Jl. Palembang-Prabumulih, Km.90-32, Ogan Ilir, South Sumatera, Indonesia
[b] Research Center Inorganic Center of Inorganic Materials and Complexes, Faculty of Mathematics and Natural Sciences, Sriwijaya University, Jl. Padang Salasa No. 524 Ilir Barat 1, Palembang 30139, South Sumatera, Indonesia

ARTICLE INFO

Keywords:
Selective
Layered double hydroxide
Charcoal activated
Direct yellow
Adsorption

ABSTRACT

In this investigation, MgAl-Charcoal activated was prepared and characterized using XRD, FTIR, BET, and SEM analyses. MgAl-Charcoal activated exhibited characteristic peaks at $2\theta = 10.85^{\circ}$ (003), 21.64° (002), 34.60° (015), and 60.65° (013). FTIR absorption spectra of MgAl-Charcoal activated typical absorption at 3448, 1635, 1381, and 601 cm^{-1}. The surface areas of MgAl, charcoal activated, and MgAl-Charcoal activated were 8.963, 757.845, and 1449.020 m^2/g, respectively. The surface area of MgAl expanded 161 times after being combined with charcoal activated. The typical MgAl, charcoal activated, and MgAl-Charcoal activated surfaces are not uniform in size and shape. MgAl and MgAl-Charcoal activated absorb direct yellow more than methyl orange and direct green. The significant drop in direct yellow concentration suggested that the direct yellow structure was smaller than methyl orange and direct green. The correlation coefficient revealed that the adsorption of direct yellow followed the pseudo-second-order and Langmuir model. The maximum adsorption of direct yellow capabilities of MgAl, charcoal activated, and MgAl-Charcoal activated were 101.010 mg/g, 71.429 mg/g, and 133.333 mg/g, respectively. In the fifth cycle, the regeneration efficiency of MgAl, charcoal activated, and MgAl-Charcoal activated decreased from 70.652 % to 29.762 %, 68.711 % to 37.785 %, and 92.003 % to 66.382 %, respectively. These findings show the effective regeneration of MgAl-Charcoal activated for adsorption of direct yellow.

1. Introduction

The release of colored effluent into recipient streams diminishes the aesthetic value of water and limits the penetration of sunlight into the water, hence diminishing its photosynthetic capabilities [1]. Colorants such as dyes are among the harmful substances discharged into the aquatic environment by many businesses, including the dye manufacturing, leather, and textile industries [2]. The presence of dyes and pigments substantially negatively impacts aquatic fauna and vegetation [3].

Direct yellow is classified as an azo dye and is utilized in various activities, including printing, coloring cellulosic fibers, and creating related combinations [4]. These direct dyes are anionic, water-soluble, and contain functional groups that react with a wide range of substances via the formation of covalent bonds, ion-exchange effect, and complexation effect [5]. Therefore, the treatment of industrial dye effluents requires practical and cost-effective methods. Dye wastewater has been treated using physicochemical methods such as photocatalytic, coagulation, biological anaerobic–aerobic, and adsorption processes [6]. Adsorption is one method for pre-concentrating pesticide residues from an aqueous medium onto a solid adsorbent material [7]. According to a report by Wang et al. [8], the adsorption capacity of bamboo charcoal for direct yellow is 2.401 mg/g. Campos et al. [9] discovered that MnS could absorb direct yellow at 58.3 mg/g. In addition, Azizi et al. [10] modified graphene oxide with adsorption capabilities of 10.71 mg/g for direct yellow adsorption. Previous research only adsorbed direct yellow without a selective dye method, although authentic wastewater dyes are frequently a mixture of various dyes. For the efficient adsorption of pesticide residues, hydrocalumite, chitosan, humic acid, montmorillonite, and layered double hydroxide [11–14] have been reported.

Layered double hydroxide (LDH) is formed from the clay mineral

* Corresponding author at: Graduate School, Faculty of Mathematics and Natural Sciences, Sriwijaya University, Jl. Palembang-Prabumulih, Km.90-32, Ogan Ilir, South Sumatera, Indonesia.
E-mail address: aldeslesbani@pps.unsri.ac.id (A. Lesbani).

https://doi.org/10.1016/j.rechem.2023.100766
Received 1 December 2022; Accepted 2 January 2023
Available online 4 January 2023

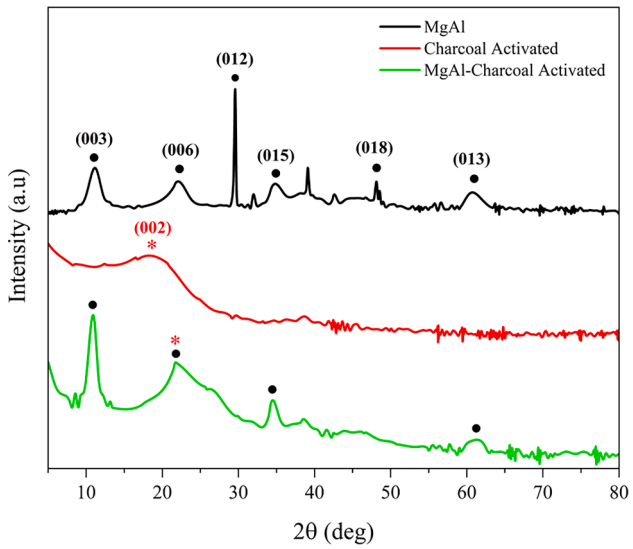

Fig. 1. XRD diffractogram of adsorbents.

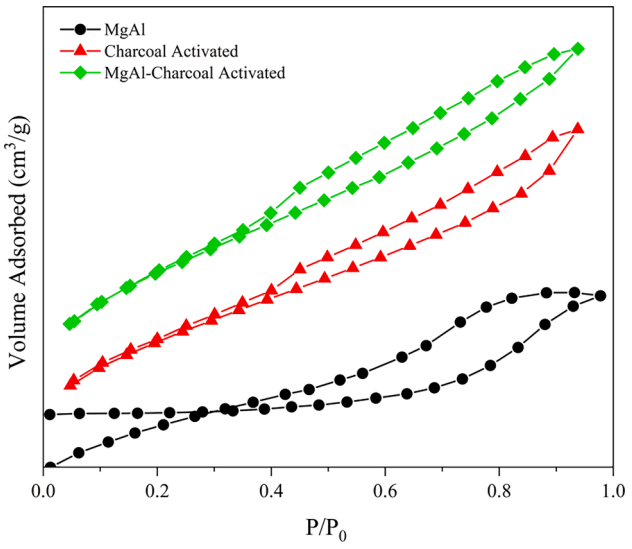

Fig. 3. N_2 adsorption–desorption isotherms of adsorbents.

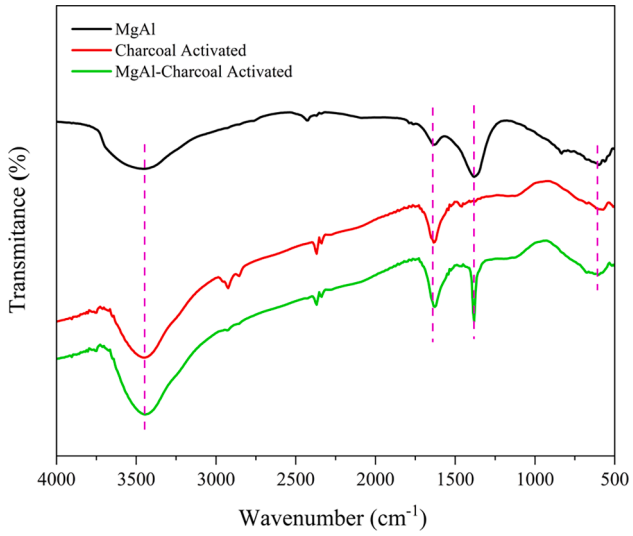

Fig. 2. IR spectra of adsorbents.

brucite [15]. Positively charged divalent (M^{2+}) and trivalent (M^{3+}) ions contribute to the structure of LDH. In the brucite production of LDH, M^{2+} is replaced by M^{3+}, giving the lamellae a positive charge [16,17]. This positive charge is neutralized by water and anions in the inter-lamellar region, promoting lamellae accumulation and the formation of an LDH structure [18]. LDH have improved adsorption efficiency due to their exceptional anion exchange capacity and large surface area [19,20]. LDH has been used for oxidative desulfurization of dibenzothiophene, heavy metals adsorption, and dye adsorption [21–23]. Nonetheless, the cycle stability and adsorption capacity of LDH-based adsorbents are inadequate [24]. Consequently, LDH was reacted with charcoal activated.

Charcoal activated has been demonstrated to be an efficient and easily produced material [25]. By burning biomass, such as bamboo, coffee bean, coconut shells, and sugarcane, to a temperature of approximately 700 °C in the absence of oxygen, charcoal can be created [26]. Charcoal activated is the most adaptable adsorbent due to its various physical and chemical features, which include a large surface area with a porous structure, exceptional adsorption capacity, and a modifiable surface chemical composition [27,28]. Therefore, layered double hydroxide was modified with charcoal activated to facilitate the

Table 1
BET results of adsorbents.

Adsorbent	Surface Area (m^2/g)	Pore Size (nm), BJH	Pore Volume (cm^3/g), BJH
MgAl	8.963	6.225	0.028
Charcoal activated	757.845	2.006	0.760
MgAl-Charcoal activated	1449.020	1.892	1.409

selective adsorption of dyes. In genuine dye wastewater, dyes are often a mixture of different dyes, depending on the manufacturing process [29]. Dyes adsorption was selective based on electrostatic interaction, size, hydrogen bonding, etc.

In this investigation, MgAl-Charcoal activated was prepared and characterized using XRD, FTIR, BET, and SEM analyses. Determine the dye that is most readily absorbed using the dye's selectivity. Mixing direct yellow, methyl orange, and direct green produced selectivity. The selective dye is followed by an adsorption process. The pH, kinetics, isotherm, thermodynamics, and adsorption process were explored as adsorption parameters.

2. Material and method

2.1. Materials and instrumentation

The nonahydrate of aluminum nitrate ($Al(NO_3)_3{\cdot}9H_2O$) was acquired from Sigma-Aldrich. The magnesium (II) nitrate hexahydrate ($Mg(NO_3)_2{\cdot}6H_2O$) and sodium hydroxide (NaOH) were supplied by EMSURE® ACS. The procurement of hydrogen chloride (HCl) from Mallinckrodt®. Charcoal activated was acquired from the Tokyo Chemical Industry. Distilled water was purchased from PT. Bratachem, Indonesia. UV–vis Spectrophotometer type Biobase BK-UV 1800 PC, Fourier Transfer Infra-Red (FTIR) type Shimadzu Prestige-21, X-ray Diffractometer (XRD) type Rigaku Miniflex-6000, N_2 adsorption–desorption isotherms analysis type Quantachrome Touchwin v1.22, and Scanning Electron Microscope (SEM) type Quanta 650 were among the analytical instruments.

2.2. Preparation of MgAl-Charcoal activated

Synthesis LDH [30]: MgAl was produced by adding 30 mL of Mg $(NO_3)_2{\cdot}6H_2O$ and 30 mL of $Al(NO_3)_3{\cdot}9H_2O$ (at a molar ratio of 3:1) to 2

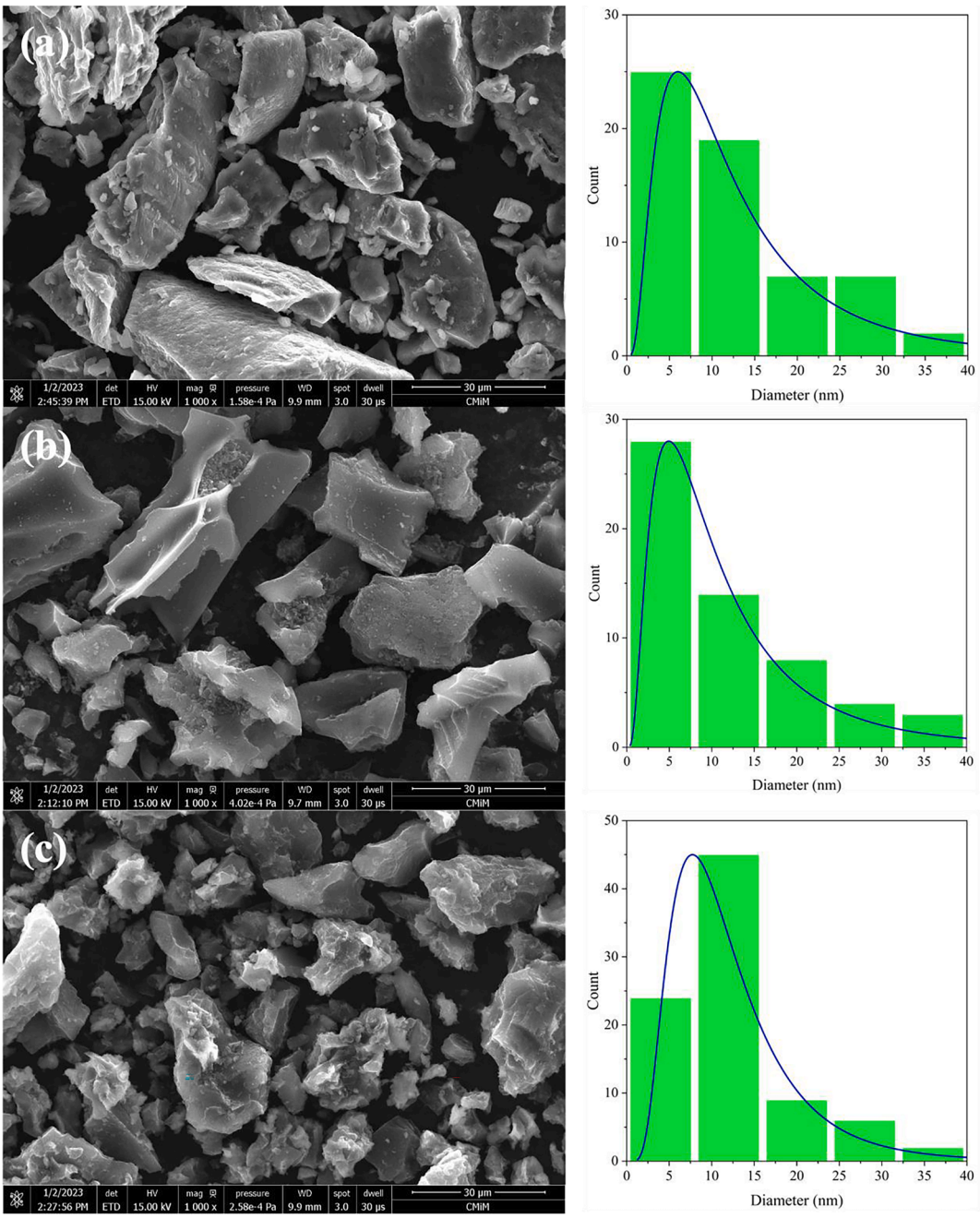

Fig. 4. SEM images and diameter distribution of MgAl (a), Charcoal activated (b), MgAl-Charcoal activated (c).

M NaOH at pH 10 and stirring for 10 h at 355 K. Thereafter, 3 g of charcoal activated was added to the MgAl, stirred continuously at 300 rpm for 72 h at 355 K, filtered, and dried. MgAl-Charcoal activated was obtained ~ 7 g.

2.4. Selective adsorption of anionic dyes

The selective adsorption of anionic dyes was determined by examining their selectivity. Direct yellow (DY, $C_{16}H_{10}N_2Na_2O_7S_2$) CAS No. 1325–37-7, methyl orange (MO, $C_{14}H_{14}N_3NaO_3S$) CAS No. 547–58-0, and direct green (DG, $C_{34}H_{21}Cl_2N_7Na_2O_8S_2$) CAS No. 6486–55-1 were mixed at a concentration of 10 mg/L, respectively. MgAl and MgAl-charcoal activated (20 mg) were added to 20 mL of dye mixture and shaken for 5, 10, 15, 20, and 25 min. Wavelength scan measured using Spectrophotometer UV–vis (350–700 nm).

2.5. Determination of pH optimum and pHpzc

The optimum pH was studied to find the most absorbing dyes. The adsorbents were applied to 20 mL of dye at different pH levels ranging from 2 to 10. To modify the initial pH, HCl 0.1 M or NaOH 0.1 M was added. The mixture was then stirred for 2 h. pHpzc was obtained using the standard pH-drift technique. 20 mg of adsorbents were added to 20 mL of 0.1 M NaCl at pH values ranging from 2 to 11. To modify the initial pH, HCl 0.1 M or NaOH 0.1 M was added. The mixture was then stirred for 24 h. Each NaCl's final pH is tested.

2.6. Adsorption of direct yellow

Adsorption parameters were investigated, such as time (0–150 min), temperature (303–323 K), and initial concentration of DY (20–100 mg/L). DY was analyzed using a spectrophotometer UV–Vis$\lambda = 398$ nm. The

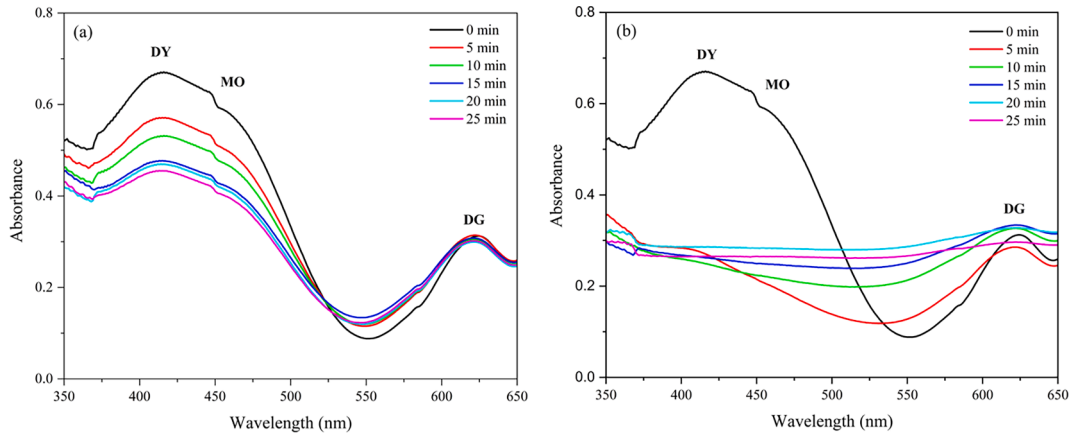

Fig. 5. Wavelength scan of anionic dyes on MgAl (a) and MgAl-Charcoal activated (b).

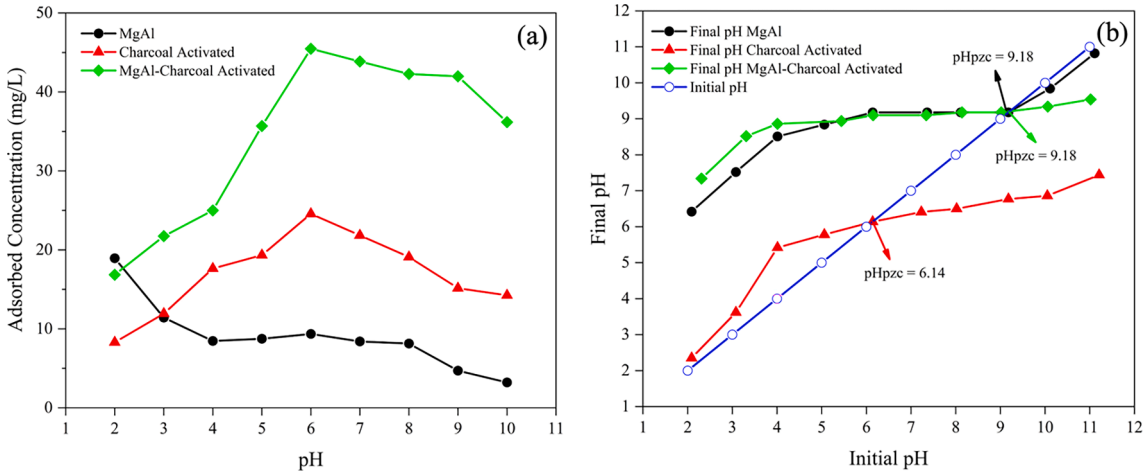

Fig. 6. Ph optimum (a) and phpzc (b) of adsorbents.

Table 2
Kinetics parameters for the adsorption of direct yellow.

Kinetic Parameter	Parameter	Adsorbent		
		MgAl	Charcoal activated	MgAl-Charcoal activated
PFO	Qe_{exp} (mg/g)	17.725	15.714	22.751
	Qe_{calc} (mg/g)	21.568	19.724	23.185
	k_1 (min^{-1})	0.025	0.027	0.022
	R^2	0.960	0.965	0.997
PSO	Qe_{exp} (mg/g)	17.725	15.714	22.751
	Qe_{calc} (mg/g)	27.778	25.189	31.447
	k_2 (g/mg.min)	0.0004	0.0005	0.0006
	R^2	0.979	0.982	0.999

adsorption capacity (Q_t) for t time (mg/g) is determined following equation:

$$Q_t = \frac{(C_0 - C_t) \times V}{W}$$

where C_0 and C_t are the initial concentration and concentration for t time of DY, respectively (mg/L); V is the volume of DY (L); W is the mass of MgAl, Charcoal activated, and MgAl-Charcoal activated, (g).

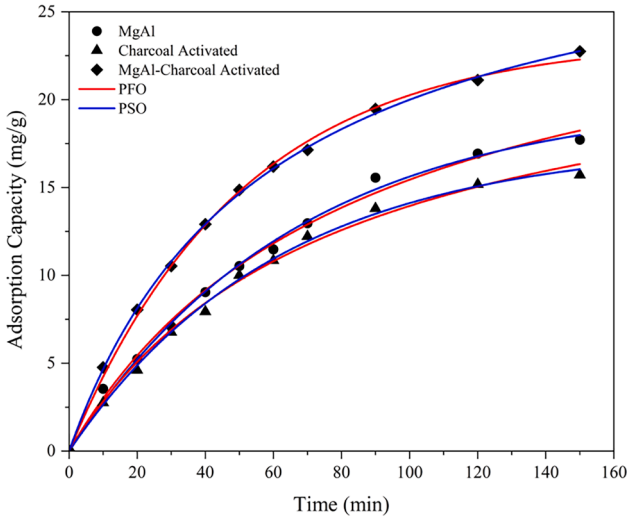

Fig. 7. Effect of contact time in adsorption of direct yellow.

3. Results and discussion

3.1. Characterization

The XRD diffractogram of MgAl from JCPDS No. 22–700 was studied

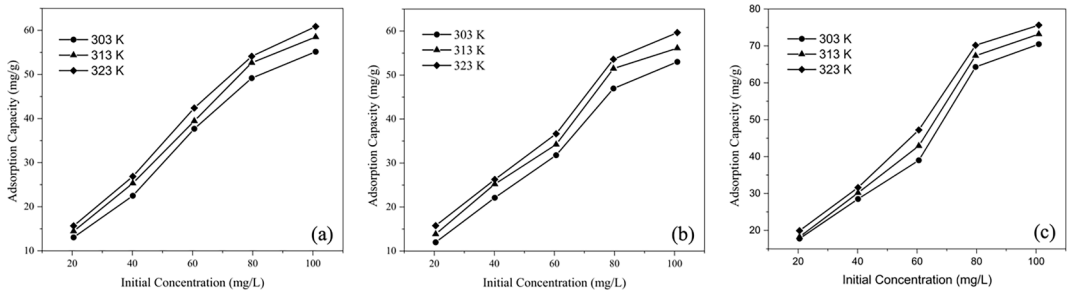

Fig. 8. Effect of initial concentration MgAl (a), charcoal activated (b), MgAl-Charcoal activated (c).

Table 3
Isotherms parameters.

Adsorbent	T (K)	Langmuir			Freundlich		
		Qmax	kL	R^2	n	kF	R^2
MgAl	303	97.087	0.030	0.924	1.110	1.972	0.850
	313	101.010	0.034	0.872	1.911	8.523	0.826
	323	92.593	0.050	0.975	1.463	5.299	0.961
Charcoal activated	303	71.429	0.022	0.993	1.120	1.750	0.969
	313	66.667	0.040	0.999	1.325	3.344	0.947
	323	54.348	0.079	0.962	1.583	5.636	0.939
MgAl-Charcoal activated	303	133.333	0.064	0.964	1.888	10.193	0.752
	313	98.039	0.101	0.941	1.883	11.719	0.773
	323	85.470	0.050	0.891	3.104	23.545	0.738

Table 4
Several adsorbents to adsorption of direct yellow.

Adsorbent	*Qmax* (mg/g)	Ref.
Zeolite	83.33	[47]
Nano bentonite	86.008	[48]
Biomass magnetic composites	119.1	[49]
Cotton fiber	83.179	[50]
Polyethyleneimine treated	65.8	[51]
ZnS: Mn nanoparticle loaded activated carbon	90.05	[52]
Activated carbon from orange peel	75.76	[53]
MgAl	101.010	This study
Charcoal activated	71.429	This study
MgAl-Charcoal activated	133.333	This study

Table 5
Adsorption thermodynamic parameter.

Adsorbent	Δ H (kJ/mol)	Δ S (J/K.mol)	Δ G (kJ/mol)			R^2
			303 K	313 K	323 K	
MgAl	9.449	0.033	−0.484	−0.812	−1.139	0.994
Charcoal activated	10.901	0.037	−0.243	−0.611	−0.978	0.996
MgAl-Charcoal activated	10.427	0.041	−2.115	−2.529	−2.943	0.999

[31]. MgAl-Charcoal activated exhibited characteristic peaks at 2θ = 10.85° (003), 21.64° (002), 34.60° (015), and 60.65° (013) (see Fig. 1). The diffraction peaks indicate crystal planes of MgAl at 2θ = 10.85° (003), 34.60 (015), and 60.65° (013) [32]. The diffraction peaks at 2θ = 21.64° (002) suggest the presence of carbon in charcoal activated and interlayer spacing from MgAl [33,34].

Fig. 2 shows FTIR absorption spectra of MgAl-Charcoal activated typical absorption at 3448, 1635, 1381, and 601 cm^{-1}. O—H stretching vibrations in the hydroxyl layer (MgAl-OH) comprised the 3448 cm^{-1} absorption band [35]. The peak at 1635 cm^{-1} is attributed to stretching the C═C bond and interlayer water in charcoal activated and MgAl, respectively [36]. The band at 1381 cm^{-1} is due to NO_3^- in the MgAl

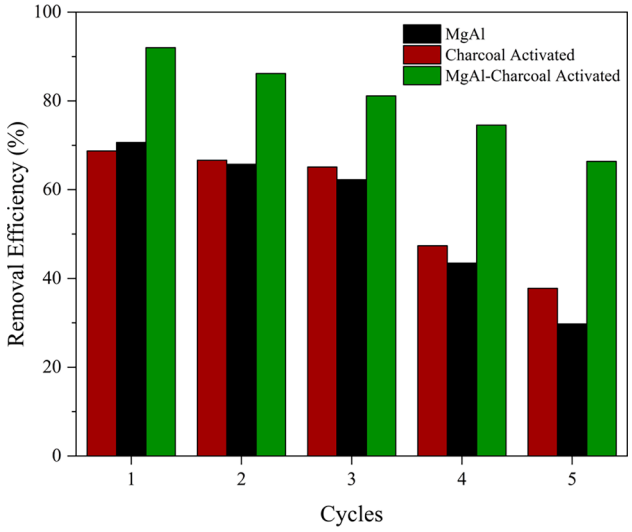

Fig. 9. Regeneration of adsorbents.

interlayer [37,38]. Al-O and Mg-O bonds in LDH are responsible for the peaks that occurred at 601 cm^{-1} [39].

Fig. 3 depicts the N_2 adsorption–desorption of MgAl, charcoal activated, and MgAl-Charcoal activated. The profile N_2 adsorption–desorption materials exhibited type IV isotherm and H3 hysteresis loop, classifying materials as having a mesoporous structure (pore size range 2–50 nm) [40,41]. Table 1 summarizes the materials' surface area, pore size, and pore volume. The surface areas of MgAl, charcoal activated, and MgAl-Charcoal activated were at 8.963, 757.845, and 1449.020 m^2/g, respectively. The surface area of MgAl expanded 161 times after being combined with charcoal activated. The pore size of materials was between 2 and 6 nm, confirming mesoporosity, and was distributed as follows: MgAl > charcoal activated > MgAl-Charcoal activated. The pore volumes of MgAl, charcoal activated, and MgAl-Charcoal activated were 0.028, 0.760, and 1.409 cm^3/g, respectively.

Fig. 4 shows the surface morphology and diameter distribution of MgAl, charcoal activated, and MgAl-Charcoal activated. The typical MgAl, charcoal activated, and MgAl-Charcoal activated surfaces are not uniform in size and shape. The average diameter distributions of MgAl, charcoal activated, and MgAl-Charcoal activated are 14.09 nm, 12.43 nm, and 12.24 nm, respectively. Compared to MgAl and charcoal activated, MgAl-Charcoal activated had a smaller diameter distribution.

3.2. Selective adsorption of anionic dyes

Wavelength scans for the selective adsorption of direct yellow (DY), methyl orange (MO), and direct green (DG) are depicted in Fig. 5. MgAl and MgAl-Charcoal activated absorb DY more than MO and DG. The significant drop in DY concentration suggested that the DY structure was smaller than MO and DG. In addition, DY in adsorbents has greater

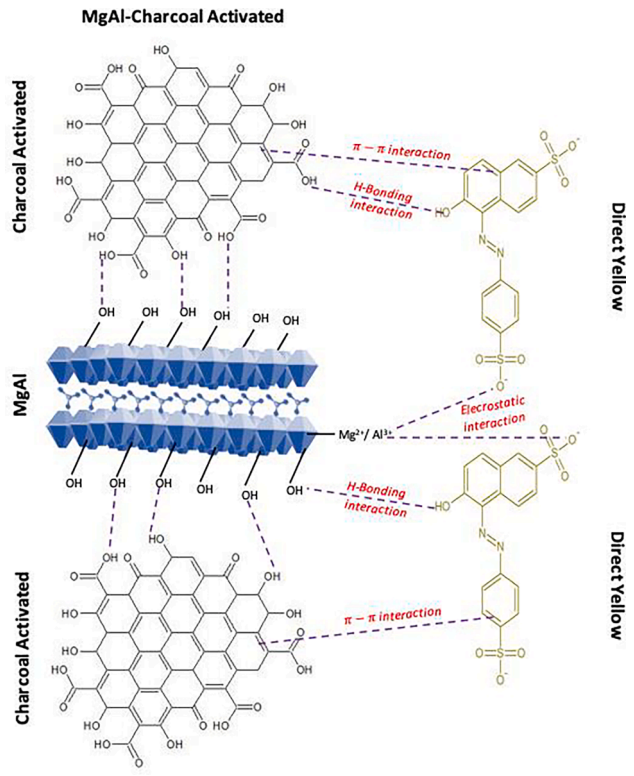

Fig. 10. Proposed adsorption mechanism of direct yellow on MgAl-Charcoal activated.

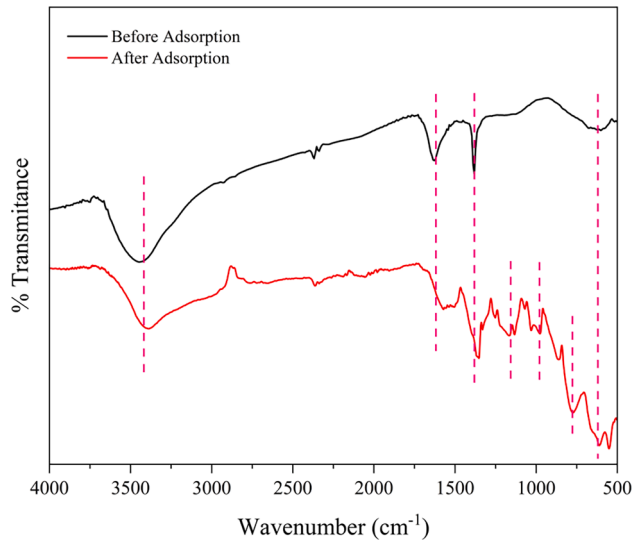

Fig. 11. IR spectra of MgAl-Charcoal activated before and after adsorption.

electrostatic interaction and hydrogen bonding than MO and DG. Consequently, direct yellow is applied in the adsorption process.

3.3. pH optimum and pHpzc

The pH impacts the degree of ionization of the dye and the surface charge of the adsorbent, which has a substantial impact on the adsorption capacity [42,43]. The effect of pH on the adsorption of direct yellow is depicted in Fig. 6a. The optimum pH of MgAl, charcoal activated, and MgAl-Charcoal activated was determined to be 2, 6, and 6, respectively. pH*pzc* is the neutral point with neither a positive nor a negative charge. There is no movement of H^+ ions at the meeting point between the initial and final pH; hence this meeting point is the pH*pzc*. As shown in Fig. 6b, the pH*pzc* of MgAl, charcoal activated, and MgAl-Charcoal activated were pH 9.18, 6.14, and 9.18, respectively. Adsorbents are positively charged in solutions with a pH lower than pH*pzc* and negatively charged in solutions with a pH greater than pH*pzc* [44].

3.4. Adsorption of direct yellow

Adsorption process considerations include the kinetic study. An excellent adsorbent has a high rate of adsorption and a high level of efficiency. The adsorption kinetics model includes pseudo-first-order (PFO) and pseudo-second-order (PSO) to demonstrate the connection between contact time and adsorption capacity. The correlation coefficients (R^2) of MgAl, charcoal activated, and MgAl-Charcoal activated at PSO > PFO are displayed in Table 2. The correlation coefficient revealed that the adsorption of direct yellow followed PSO (see Fig. 7). PSO indicated that chemisorption might be the dominant adsorption [45].

The isotherms study investigates the mechanism of adsorbent-adsorbate interaction. In process adsorption, the isotherm parameter can be studied using a variety of initial concentrations and temperatures (See Fig. 8). The Langmuir and Freundlich model was applied for this study's adsorption isotherm. Table 3 displays the correlation coefficients of MgAl, charcoal activated, and MgAl-Charcoal activated at Langmuir > Freundlich. The correlation coefficient value indicated that the adsorption of direct yellow follows the Langmuir isotherm, which entails monolayer adsorption with evenly distributed active sites on the surface of the adsorbent [46]. The maximum adsorption of direct yellow capabilities of MgAl, charcoal activated, and MgAl-Charcoal activated were 101.010 mg/g, 71.429 mg/g, and 133.333 mg/g, respectively. Table 4 compares the adsorption of direct yellow by various adsorbents.

The thermodynamics study investigated adsorption's spontaneity and heat changes. The positive value of ΔH in Table 5 implies that the adsorption is endothermic [54]. When adsorption occurs on adsorbents, ΔS is a spontaneously positive value showing an increase in the degrees of freedom of the direct yellow [55]. ΔG is negative, indicating that spontaneous adsorption of direct yellow occurs. As the temperature rises, the growing negative value of ΔG shows that the adsorption process is more spontaneous [56,57]. Fig. 9 depicts the regeneration of MgAl, charcoal activated, and MgAl-Charcoal activated in direct yellow adsorption–desorption cycles. In the fifth cycle, the regeneration efficiency of MgAl, charcoal activated, and MgAl-Charcoal activated decreased from 70.652 % to 29.762 %, 68.711 % to 37.785 %, and 92.003 % to 66.382 %, respectively. These findings show the effective regeneration of MgAl-Charcoal activated for adsorption of direct yellow.

The proposed adsorption mechanism of direct yellow on MgAl-Charcoal activated is represented in Fig. 10. pH*pzc* can show the mechanism for adsorption of direct yellow [58]. pH*pzc* (point zero charges) of MgAl, charcoal activated, and MgAl-Charcoal activated were pH 9.18, 6.14, and 9.18. Meanwhile, the optimum pH was at 2, 6, and 6, respectively. When the optimum pH = pH*pzc*, only physical adsorption occurs; when the optimum pH ≠ pH*pzc*, both physical and chemical adsorption occurs. In this study, the optimum pH < pH*pzc* on MgAl, charcoal activated, and MgAl-Charcoal activated to indicate that chemical and physical adsorption occur, and the adsorbent surface is Mg^{2+} and Al^{3+} in LDH, resulting in a positive charge that will interact electrostatically with the anionic of direct yellow. Additionally, hydrogen bonding and π-π interactions in the aromatic ring in direct yellow and adsorbent might influence the adsorption mechanism. As displayed in Fig. 11, IR spectra after adsorption support the adsorption mechanism. The new peaks at 783 and 979 cm^{-1} indicated electrostatic interaction between MgAl-Charcoal activated and direct yellow. In addition, the new peak at 1163 cm^{-1} suggested S—O stretch vibration from direct yellow.

4. Conclusion

Preparation of MgAl-Charcoal activated was successful with characterized using XRD, FTIR, BET, and SEM analyses. Selective adsorption of anionic dyes shows that direct yellow is more selective than methyl orange and direct green. Adsorption of direct yellow on MgAl-Charcoal activated has a maximum adsorption capacity of 133.333 mg/g. In the fifth cycle, the regeneration efficiency of MgAl-Charcoal activated decreased from 92.003 % to 66.382 %. These findings show the effective regeneration of MgAl-Charcoal activated for adsorption of direct yellow. p*Hpzc* can establish the mechanism for the adsorption of direct yellow. Electrostatic interaction, hydrogen bonding interactions, and π-π interactions in direct yellow and adsorbent might influence the adsorption mechanism.

CRediT authorship contribution statement

Nur Ahmad: Conceptualization, Investigation, Writing – original draft, Software. **Fitri Suryani Arsyad:** Methodology, Validation, Visualization. **Idha Royani:** Visualization, Data curation, Formal analysis. **Aldes Lesbani:** Methodology, Conceptualization, Writing – review & editing, Supervision.

Declaration of Competing Interest

The authors declare that they have no known competing financial interests or personal relationships that could have appeared to influence the work reported in this paper.

Data availability

No data was used for the research described in the article.

Acknowledgement

The author thanks to Research Center of Inorganic Materials and Complexes Universitas Sriwijaya for laboratory analysis and support.

References

[1] E.A. Alabbad, S. Bashir, J.L. Liu, Efficient removal of direct yellow dye using chitosan crosslinked isovanillin derivative biopolymer utilizing triboelectric energy produced from homogeneous catalysis, Catal. Today (2021), https://doi.org/10.1016/j.cattod.2021.06.017.

[2] F. Ali, S. Bibi, N. Ali, Z. Ali, A. Said, Z.U. Wahab, M. Bilal, H.M.N. Iqbal, Sorptive Removal of Malachite Green Dye by Activated Charcoal: Process Optimization, Kinetic, and Thermodynamic Evaluation, Case Studies in Chem. Environ. Eng. 2 (2020), https://doi.org/10.1016/j.cscee.2020.100025.

[3] M. Ghaedi, A. Ansari, R. Sahraei, ZnS: Cu nanoparticles loaded on activated carbon as novel adsorbent for kinetic, thermodynamic and isotherm studies of Reactive Orange 12 and Direct yellow 12 adsorption, Spectrochim. Acta A Mol. Biomol. Spectrosc. 114 (2013) 687–694, https://doi.org/10.1016/j.saa.2013.04.091.

[4] M. Wawrzkiewicz, E. Polska-Adach, Z. Hubicki, Polacrylic and polystyrene functionalized resins for direct dye removal from textile effluents, Separation Science and Technology (Philadelphia). 55 (2020) 2122–2136, https://doi.org/10.1080/01496395.2019.1583254.

[5] S. Yao, M. Fabbricino, L. Pontoni, M. Race, F. Parrino, L. Savignano, G. D'Errico, Y. Chen, Characterization of anthropogenic organic matter and its interaction with direct yellow 27 in wastewater: Experimental results and perspectives of resource recovery, Chemosphere 286 (2022), https://doi.org/10.1016/j.chemosphere.2021.131528.

[6] M. Zabihi, A. Motavalizadehkakhky, PbS/ZIF-67 nanocomposite: novel material for photocatalytic degradation of basic yellow 28 and direct blue 199 dyes, J. Taiwan Inst. Chem. Eng. 140 (2022), https://doi.org/10.1016/j.jtice.2022.104572.

[7] A.A. Mir, A.A. Amooey, S. Ghasemi, Adsorption of direct yellow 12 from aqueous solutions by an iron oxide-gelatin nanoadsorbent; kinetic, isotherm and mechanism analysis, J. Clean. Prod. 170 (2018) 570–580, https://doi.org/10.1016/j.jclepro.2017.09.101.

[8] L.G. Wang, G.B. Yan, Adsorptive removal of direct yellow 161dye from aqueous solution using bamboo charcoals activated with different chemicals, Desalination 274 (2011) 81–90, https://doi.org/10.1016/j.desal.2011.01.082.

[9] A.F.C. Campos, P.H. Michels-Brito, F.G. da Silva, R.C. Gomes, G. Gomide, J. Depeyrot, Removal of direct yellow 12 from water using CTAB-coated core-shell bimagnetic nanoadsorbents, J. Environ. Chem. Eng. 7 (2019), https://doi.org/10.1016/j.jece.2019.103031.

[10] A. Azizi, E. Moniri, A.H. Hassani, H.A. Panahi, M. Jafarinezhad, Nonlinear and linear analysis of Direct Yellow 50 adsorption onto modified graphene oxide: Kinetic, isotherm, and thermodynamic studies, Desalination, Water Treat. 229 (2021) 352–361, https://doi.org/10.5004/dwt.2021.27362.

[11] H. Li, L. Miao, G. Zhao, W. Jia, Z. Zhu, Preparation of high-performance chitosan adsorbent by cross-linking for adsorption of Reactive Red 2 (RR2) dye wastewater, J. Environ. Chem. Eng. 10 (2022), https://doi.org/10.1016/j.jece.2022.108872.

[12] I. Chouaybi, H. Ouassif, M. Bettach, E.M. Moujahid, Fast and high removal of acid red 97 dye from aqueous solution by adsorption onto a synthetic hydrocalumite: Structural characterization and retention mechanisms, Inorg. Chem. Commun. 146 (2022), 110169, https://doi.org/10.1016/j.inoche.2022.110169.

[13] N. Ahmad, F. Suryani Arsyad, I. Royani, A. Lesbani, Selectivity of Malachite Green on Cationic Dye Mixtures Toward Adsorption on Magnetite Humic Acid, Environ. Nat. Resour. J. 20 (2022) 1–10, https://doi.org/10.32526/ennrj/20/202200142.

[14] T. Taher, R. Putra, N. Rahayu Palapa, A. Lesbani, Preparation of magnetite-nanoparticle-decorated NiFe layered double hydroxide and its adsorption performance for congo red dye removal, Chem. Phys. Lett. 777 (2021), 138712, https://doi.org/10.1016/j.cplett.2021.138712.

[15] H.D. Güzel, M. Çalışkan, T. Baran, Supported Pd nanoparticles on micro structured chitosan-MgAl layered double hydroxide hydrogel beads as a sustainable, effective, and recyclable nanocatalyst for Heck cross-coupling reactions, J. Phys. Chem. Solid 167 (2022), https://doi.org/10.1016/j.jpcs.2022.110777.

[16] T. van Everbroeck, J. Wu, D. Arenas-Esteban, R.-G. Ciocarlan, M. Mertens, S. Bals, C. Dujardin, P. Granger, E.M. Seftel, P. Cool, ZnAl layered double hydroxide based catalysts (with Cu, Mn, Ti) used as noble metal-free three-way catalysts, Appl. Clay Sci. 217 (2022), 106390, https://doi.org/10.1016/j.clay.2021.106390.

[17] Y. Wang, Z. Zhang, S. Wang, M. Han, Integration of MgAl-layered double hydroxides into TiO2 nanorods as photoanodes for enhanced photoelectrochemical water splitting, Catal. Commun. 164 (2022), https://doi.org/10.1016/j.catcom.2022.106434.

[18] H. Lv, H. Rao, Z. Liu, Z. Zhou, Y. Zhao, H. Wei, Z. Chen, NiAl layered double hydroxides with enhanced interlayer spacing via ion-exchange as ultra-high performance supercapacitors electrode materials, J Energy Storage. 52 (2022), https://doi.org/10.1016/j.est.2022.104940.

[19] X. Pan, M. Zhang, H. Liu, S. Ouyang, N. Ding, P. Zhang, Adsorption behavior and mechanism of acid orange 7 and methylene blue on self-assembled three-dimensional MgAl layered double hydroxide: Experimental and DFT investigation, Appl. Surf. Sci. 522 (2020), https://doi.org/10.1016/j.apsusc.2020.146370.

[20] X. Luo, Z. Huang, J. Lin, X. Li, J. Qiu, J. Liu, X. Mao, Hydrothermal carbonization of sewage sludge and in-situ preparation of hydrochar/MgAl-layered double hydroxides composites for adsorption of Pb(II), J. Clean. Prod. 258 (2020), https://doi.org/10.1016/j.jclepro.2020.120991.

[21] D. Brahma, H. Saikia, Synthesis of ZrO2/MgAl-LDH composites and evaluation of its isotherm, kinetics and thermodynamic properties in the adsorption of congo red dye, Chemical Thermodynamics and Thermal, Analysis (2022), 100067, https://doi.org/10.1016/j.ctta.2022.100067.

[22] N. Ahmad, A. Wijaya, E. Salasia Fitri, F. Suryani Arsyad, R. Mohadi, A. Lesbani, Catalytic Oxidative Desulfurization of Dibenzothiophene by Composites Based Ni/Al-Oxide, 2022. https://doi.org/11.26554/sti.2222.7.3.385-391.

[23] Q. Huang, Y. Chen, H. Yu, L. Yan, J. Zhang, B. Wang, B. Du, L. Xing, Magnetic graphene oxide/MgAl-layered double hydroxide nanocomposite: One-pot solvothermal synthesis, adsorption performance and mechanisms for Pb2+, Cd2+, and Cu2+, Chem. Eng. J. 341 (2018) 1–9, https://doi.org/10.1016/j.cej.2018.01.156.

[24] H.P. Utami, N. Ahmad, Z.A. Zahara, A. Lesbani, R. Mohadi, Green Synthesis of Nickel Aluminum Layered Double Hydroxide using Chitosan as Template for Adsorption of Phenol, 2022. https://doi.org/11.26554/sti.2222.7.4.533-535.

[25] J. Shen, G. Huang, C. An, X. Xin, C. Huang, S. Rosendahl, Removal of Tetrabromobisphenol A by adsorption on pinecone-derived activated charcoals: Synchrotron FTIR, kinetics and surface functionality analyses, Bioresour. Technol. 247 (2018) 812–820, https://doi.org/10.1016/j.biortech.2017.09.177.

[26] R. Thotagamuge, M.R.R. Kooh, A.H. Mahadi, C.M. Lim, M. Abu, A. Jan, A.H. A. Hanipah, Y.Y. Khiong, A. Shofry, Copper modified activated bamboo charcoal to enhance adsorption of heavy metals from industrial wastewater, Environ. Nanotechnol. Monit. Manag. 16 (2021), https://doi.org/10.1016/j.enmm.2021.100562.

[27] B. Ekka, I. Mierina, T. Juhna, K. Kokina, M. Turks, Synergistic effect of activated charcoal and chitosan on treatment of dairy wastewaters, Mater. Today Commun. 31 (2022), https://doi.org/10.1016/j.mtcomm.2022.103477.

[28] S.S. Nayak, N.A. Mirgane, V.S. Shivankar, K.B. Pathade, G.C. Wadhawa, Adsorption of methylene blue dye over activated charcoal from the fruit peel of plant hydnocarpus pentandra, in: Mater Today Proc, Elsevier Ltd, 2020, pp. 2302–2305, https://doi.org/10.1016/j.matpr.2020.07.728.

[29] Y. Shi, Q. Chang, T. Zhang, G. Song, Y. Sun, G. Ding, A review on selective dye adsorption by different mechanisms, J. Environ. Chem. Eng. 10 (2022), 108639, https://doi.org/10.1016/j.jece.2022.108639.

[30] N. Juleanti, N. Normah, P.M.S.B.N. Siregar, A. Wijaya, N.R. Palapa, T. Taher, N. Hidayati, R. Mohadi, A. Lesbani, Comparison of the Adsorption Ability of MgAl-HC, CaAl-HC, and ZaAl-HC Composite Materials Based on Duku Peel Hydrochar in Adsorption of Direct Green Anionic Dyes, Indonesian, J. Chem. 22 (2022) 192–204, https://doi.org/10.22146/ijc.68719.

[31] G. Buema, N. Lupu, H. Chiriac, G. Ciobanu, O. Kotova, M. Harja, Modeling of solid-fluid non-catalytic processes for nickel ion removal, Rev. Chim. 71 (2020) 4–15, https://doi.org/10.37358/RC.20.7.8221.

[32] C.T. Vu, T. Wu, MgAl-layered double hydroxides/sodium alginate beads for nitrate adsorption from groundwater and potential use as a slow-release fertilizer, J. Clean. Prod. 379 (2022), https://doi.org/10.1016/j.jclepro.2022.134508.
[33] H.N. Tran, D.T. Nguyen, G.T. Le, F. Tomul, E.C. Lima, S.H. Woo, A.K. Sarmah, H. Q. Nguyen, P.T. Nguyen, D.D. Nguyen, T.V. Nguyen, S. Vigneswaran, D.V.N. Vo, H. P. Chao, Adsorption mechanism of hexavalent chromium onto layered double hydroxides-based adsorbents: A systematic in-depth review, J. Hazard. Mater. 373 (2019) 258–270, https://doi.org/10.1016/j.jhazmat.2019.03.018.
[34] H. el Farissi, R. Lakhmiri, A. Albourine, M. Safi, O. Cherkaoui, Adsorption study of charcoal of cistus ladaniferus shell modified by H3PO4 and NaOH used as a low-cost adsorbent for the removal of toxic reactive red 23 dye: Kinetics and thermodynamics, in: Mater Today Proc, Elsevier Ltd, 2020, pp. 1740–1748, https://doi.org/10.1016/j.matpr.2020.10.438.
[35] D. Gherca, A.I. Borhan, M.M. Mihai, D.D. Herea, G. Stoian, T. Roman, H. Chiriac, N. Lupu, G. Buema, Magnetite-induced topological transformation of 3D hierarchical MgAl layered double hydroxides to highly dispersed 2D magnetic hetero-nanosheets for effective removal of cadmium ions from aqueous solutions, Mater. Chem. Phys. 284 (2022), https://doi.org/10.1016/j.matchemphys.2022.126047.
[36] J. Sun, Y. Wang, Y. He, J. Liu, L. Xu, Z. Zeng, Y. Song, J. Qiu, Z. Huang, L. Cui, Effective removal of nanoplastics from water by cellulose/MgAl layered double hydroxides composite beads, Carbohydr. Polym. 298 (2022), https://doi.org/10.1016/j.carbpol.2022.120059.
[37] Y. Chen, L. Wu, W. Yao, J. Wu, Y. Yuan, B. Jiang, F. Pan, Growth behavior and corrosion resistance of graphene oxide/MgAl Layered double hydroxide coating grown on micro-arc oxidation film of magnesium alloys, J. Ind. Eng. Chem. (2022), https://doi.org/10.1016/j.jiec.2022.10.020.
[38] S. Intasa-ard, M. Ogawa, Simple and cost-effective mass production of nitrate type MgAl layered double hydroxide: Titration from concentrated solution, Appl. Clay Sci. 228 (2022), https://doi.org/10.1016/j.clay.2022.106615.
[39] T.S. Silva, E.P. Fernandes, M. Vithanage, S.M.P. Meneghetti, L. Meili, A facile synthesis of MgAl/layered double hydroxides from aluminum wastes, Mater. Lett. 324 (2022), https://doi.org/10.1016/j.matlet.2022.132624.
[40] Y. Li, M. Wu, J. Wu, Y. Wang, Z. Zheng, Z. Jiang, Mechanistic insight and rapid co-adsorption of nitrogen pollution from micro-polluted water over MgAl-layered double hydroxide composite based on zeolite, Sep. Purif. Technol. 297 (2022), https://doi.org/10.1016/j.seppur.2022.121484.
[41] Y. Kim, Y. Son, S. Bae, T.H. Kim, Y. Hwang, Particle size and interlayer anion effect on chromate adsorption by MgAl-layered double hydroxide, Appl. Clay Sci. 225 (2022), https://doi.org/10.1016/j.clay.2022.106552.
[42] A. Li, Y. Zhang, W. Ge, Y. Zhang, L. Liu, G. Qiu, Removal of heavy metals from wastewaters with biochar pyrolyzed from MgAl-layered double hydroxide-coated rice husk: Mechanism and application, Bioresour. Technol. 347 (2022), https://doi.org/10.1016/j.biortech.2021.126425.
[43] L. Yang, J. Chen, Y. Nie, C. Shi, Q. Wang, Effective utilization of calcined MgAl-layered double hydroxides for adsorption of gold (I) thiosulfate complexes, J. Environ. Chem. Eng. 9 (2021), https://doi.org/10.1016/j.jece.2021.105273.
[44] N. Ahmad, F. Suryani Arsyad, I. Royani, A. Lesbani, Adsorption of methylene blue on magnetite humic acid: Kinetic, isotherm, thermodynamic, and regeneration studies, Results Chem. 4 (2022), 100629, https://doi.org/10.1016/j.rechem.2022.100629.
[45] H. Wu, T. Xia, L. Yin, Y. Ji, Adsorption of iodide from an aqueous solution via calcined magnetite-activated carbon/MgAl-layered double hydroxide, Chem. Phys. Lett. 774 (2021), https://doi.org/10.1016/j.cplett.2021.138612.
[46] G.E. de Souza, A.H. dos Santos, J.L.S. Ide, G. Duarte, A.O.S. McKay, L.M. Silva, Adsorption of anti-inflammatory drug diclofenac by MgAl/layered double hydroxide supported on Syagrus coronata biochar, Powder Technol. 364 (2020) 229–240, https://doi.org/10.1016/j.powtec.2020.01.083.
[47] E.A. Alabbad, Efficacy assessment of natural zeolite containing wastewater on the adsorption behaviour of Direct Yellow 50 from; equilibrium, kinetics and thermodynamic studies, Arab. J. Chem. 14 (2021), https://doi.org/10.1016/j.arabjc.2021.103041.
[48] A.S. Mahmoud, Effect of nano bentonite on direct yellow 50 dye removal; Adsorption isotherm, kinetic analysis, and thermodynamic behavior, Prog. React. Kinet. Mech. 47 (2022), https://doi.org/10.1177/14686783221090377.
[49] A. Jabeen, H.N. Bhatti, Adsorptive removal of reactive green 5 (RG-5) and direct yellow 50 (DY-50) from simulated wastewater by Mangifera indica seed shell and its magnetic composite: Batch and Column study, Environ. Technol. Innov. 23 (2021), https://doi.org/10.1016/j.eti.2021.101685.
[50] L.F.M. Ismail, H.B. Sallam, S.A. Abo Farha, A.M. Gamal, G.E.A. Mahmoud, Adsorption behaviour of direct yellow 50 onto cotton fiber: Equilibrium, kinetic and thermodynamic profile, Spectrochim. Acta A Mol. Biomol. Spectrosc. 131 (2014) 657–666, https://doi.org/10.1016/j.saa.2014.03.060.
[51] S. Sadaf, H.N. Bhatti, S. Nausheen, M. Amin, Application of a novel lignocellulosic biomaterial for the removal of Direct Yellow 50 dye from aqueous solution: Batch and column study, J. Taiwan Inst. Chem. Eng. 47 (2015) 160–170, https://doi.org/10.1016/j.jtice.2014.10.001.
[52] S. Hajati, M. Ghaedi, F. Karimi, B. Barazesh, R. Sahraei, A. Daneshfar, Competitive adsorption of Direct Yellow 12 and Reactive Orange 12 on ZnS: MN nanoparticles loaded on activated carbon as novel adsorbent, J. Ind. Eng. Chem. 20 (2014) 564–571, https://doi.org/10.1016/j.jiec.2013.05.015.
[53] A. Khaled, A. el Nemr, A. El-Sikaily, O. Abdelwahab, Treatment of artificial textile dye effluent containing Direct Yellow 12 by orange peel carbon, DES. 238 (2009) 210–232, https://doi.org/10.1016/j.desal.200.
[54] N. Li, Z. Chang, H. Dang, Y. Zhan, J. Lou, S. Wang, S. Attique, W. Li, H. Zhou, C. Sun, Deep eutectic solvents assisted synthesis of MgAl layered double hydroxide with enhanced adsorption toward anionic dyes, Colloids Surf A Physicochem Eng Asp 591 (2020), https://doi.org/10.1016/j.colsurfa.2020.124507.
[55] P. Lyu, G. Wang, B. Wang, Q. Yin, Y. Li, N. Deng, Adsorption and interaction mechanism of uranium (VI) from aqueous solutions on phosphate-impregnation biochar cross-linked Mg–Al layered double-hydroxide composite, Appl. Clay Sci. 209 (2021), https://doi.org/10.1016/j.clay.2021.106146.
[56] R. Zhu, J. Xia, H. Zhang, F. Kong, X. Hu, Y. Shen, W.H. Zhang, Synthesis of magnetic activated carbons from black liquor lignin and Fenton sludge in a one-step pyrolysis for methylene blue adsorption, J. Environ. Chem. Eng. 9 (2021), https://doi.org/10.1016/j.jece.2021.106538.
[57] K. Saini, A. Sahoo, B. Biswas, A. Kumar, T. Bhaskar, Preparation and characterization of lignin-derived hard templated carbon(s): Statistical optimization and methyl orange adsorption isotherm studies, Bioresour. Technol. 342 (2021), https://doi.org/10.1016/j.biortech.2021.125924.
[58] A.A. Ahmad, M.A. Ahmad, N.K.E.M. Yahaya, J. Karim, Adsorption of malachite green by activated carbon derived from gasified Hevea brasiliensis root, Arab. J. Chem. 14 (2021), 103104, https://doi.org/10.1016/j.arabjc.2021.103104.